Anisotropy of acoustooptic figure of merit in KH_2PO_4 crystals

Mys O., Krupych O. and Vlokh R.

Vlokh Institute of Physical Optics, 23 Dragomanov Street, 79005 Lviv, Ukraine, mys@ifo.lviv.ua

Received: 15.03.2017

Abstract. We have analyzed the anisotropy of acoustooptic figure of merit M_2 for KH_2PO_4 crystals. Basing on our results, the highest M_2 coefficient, 7.1×10^{-15} s^3/kg, is achieved for the case of isotropic acoustooptic interaction. Then the optical wave, which is polarized in the XY plane and propagates along the direction [$\bar{1}10$], interacts with the longitudinal acoustic wave propagating in the same plane along [110]. For the case of anisotropic interactions, the maximum M_2 value is smaller, 5.3×10^{-15} s^3/kg. Then the slow transverse acoustic wave propagating in the XZ or YZ planes close to the X axis interacts with the optical wave propagating close to the optic axis.

Keywords: anisotropy, acoustooptic figure of merit, acoustic wave velocity, elastooptic coefficients, KH_2PO_4 crystals, acoustooptic tunable filters

PACS: 78.20.hb, 78.20.Ci, 42.70.-a, 85.60.-q
UDC: 535.42+ 535.012.21+ 535.551

1. Introduction

KH_2PO_4 (or simply KDP) crystals are widely known as an efficient electrooptic and nonlinear optic material. At the room temperature these crystals belong to tetragonal system, being characterized with the point symmetry group $\bar{4}2m$. At the Curie point T_C = 122 K, KDP manifests a ferroelectric phase transition with the change of point symmetry $\bar{4}2m\,F\,mm2$ [1]. High electrooptic and nonlinear optical parameters of KDP, together with its wide transparency range stretching deep into the ultraviolet region, stipulates its applications for laser frequency conversion, electrooptic modulation and optical switching in different spectral regions. The ability of KDP to withstand repeated exposures of high-power laser radiation, without damages, strains or subsequent inhomogeneities in the refractive index, allows for its use for operating high-pulse laser energies [2, 3]. Actually, the nonlinear optical cells that utilize the KDP crystals seem to remain the only solution for the harmonics generation with the highest-intensity femtosecond Ti:sapphire lasers generating wide (> 30 mm) diameter beams and sub-terawatt or even terawatt peak power pulses [4–8].

Recently acoustooptic (AO) properties of KDP have attracted considerable attention associated with its utilization as a material for tunable AO filters [9–12], including those that work in the ultraviolet region. The devices of this type are used in many branches of technology and science, in particular in the LIDAR systems for monitoring ozone layer state and atmosphere pollution level [13–17]. It is known that AO figure of merit (AOFM) of a material is the main parameter that determines the efficiency of AO device based on that material. Unfortunately, the AOFM of the KDP crystals (4.6×10^{-15} s^3/kg) is not high enough if compared with the known AO crystals [11, 18]. On the other hand, we believe that the knowledge about the anisotropy of acoustic, elastooptic and elastic properties of any crystalline material can enable a conspicuous increase in its AOFM and so improving of the efficiency of AO devices based on this working material As far as we know, there is little information about this anisotropy for KDP. All of the data available in the literature have dealt with the properties only in the principal crystallographic planes.

Recently we have developed a general method that allows for determining those directions of propagation and polarization of the optical and acoustic waves (AWs) which ensure maximal AOFM magnitudes [19–25]. In particular, TeO_2, $LiNbO_3$, α-BaB_2O_4, $NaBi(MoO_4)_2$ and some others crystals have been studied as examples. In the present work we analyze the AOFM anisotropy for the KDP crystals and search for the geometries of AO interactions that reveal the highest AOFMs.

2. Background of the analytical analysis

KDP crystals are optically uniaxial and negative (n_o = 1.5073 and n_e = 1.4668 [26]) at the room temperature. As for the materials belonging to the point symmetries 4/mmm, 422, $\bar{4}2m$ and 4mm, the elastic stiffness tensor for KDP contains six independent components $C_{11} = C_{22}$, $C_{12} = C_{21}$, $C_{13} = C_{23} = C_{31} = C_{32}$, C_{33}, $C_{44} = C_{55}$ and $C_{66} \neq (C_{11} - C_{12})/2$, where a standard Voigt notation is accepted. The elastooptic tensor contains seven independent coefficients $p_{11} = p_{22}$, $p_{12} = p_{21}$, $p_{13} = p_{23}$, $p_{31} = p_{32}$, p_{33}, $p_{44} = p_{55}$ and $p_{66} \neq (p_{11} - p_{12})/2$ [27].

To study the anisotropy of AOFM for the KDP crystals, we use the method developed in our recent works [19, 20, 24, 28]. In frame of this method, the anisotropy of AOFM is analyzed issuing from the anisotropy of acoustic and elastooptic properties of a material, using the well-known relation [29]

$$M_2 = n_i^3 n_d^3 p_{ef}^2 / \rho v^3 . \quad (1)$$

In Eq. (1), n_i and n_d are the refractive indices of the incident and diffracted optical waves, p_{ef} denotes the effective elastooptic coefficient (EEC), v the phase AW velocity, and ρ the material density ($\rho = 2338$ kg/m^3 [30]). The refractive indices and the EEC in the anisotropic media depend on the propagation direction and the polarization of the both incident and diffracted optical waves. In our works [19–21, 23–25] we have discussed in detail the relations for the EECs for nine possible types of AO interactions, including six isotropic interaction types and three anisotropic ones. Like TeO_2, the KDP crystals are tetragonal and, therefore, one can make use of the p_{ef} formulae taken from Refs. [20, 21].

The anisotropy of the acoustic wave velocities can be analyzed basing on a standard Christoffel equation [31],

$$C_{ijkl} m_j m_k p_l = \rho v^2 p_l , \quad (2)$$

where C_{ijkl}, m_j and p_l denote the components of the elastic stiffness tensor, the unit wave vector of the AW and the unit displacement vector, respectively. The phase velocities are given by the eigenvalues of Eq. (2). It follows from Eq. (2) that three AWs with mutually orthogonal displacement vectors can propagate along a given direction. In order to study the anisotropy of the acoustic properties, it is necessary to consider the anisotropy of these properties in the main *ZX* crystallographic plane, which will be taken below as the starting interaction plane of the optical and acoustic wave. After that we rotate our interaction plane around *Z* and *X* axis (see, e.g., Refs. [23–25]). For the interaction planes rotated by some angle φ_Z around the *Z* axis or by φ_X

around the X axis (i.e., in the new coordinate system $X'Y'Z$), the structure of the elastic stiffness tensor is changed. The actual components of this tensor can be determined after rewriting it in the new coordinate system, according to a known procedure [27]. Then the Christoffel tensor becomes more complicated and the AW velocities can be obtained using standard numeric techniques. Notice that, for all of the point groups 4/mmm, 422, $\bar{4}2m$ and 4mm, the coordinate system XYZ is associated with the eigenvectors of the optical impermeability tensor, which coincides with the crystallographic system *abc*.

For efficient practical applications of AO materials, it is also important to know the obliquity of the acoustic energy-flow direction with respect to the AW vector. In the principal crystallographic planes , the angle between the directions of the energy flow and the AW vector can be calculated as [32]

$$\tan(\Delta) = \frac{1}{v(\Theta)} \frac{\partial v}{\partial \Theta}, \quad (3)$$

where $\Delta = \Theta - \psi$, Θ is the angle between the principal axis (e.g., the X axis) and the AW vector, ψ the angle between the crystallographic axis and the acoustic energy flow direction, and $v(\Theta)$ the AW velocity specified for the propagation direction under interest. Finally, the changes $v(\Theta)$ in the AW velocity caused by changing propagation direction can also be obtained from the Christoffel equation.

In our calculations we have used the elastic stiffness coefficients of KDP obtained in the study [33] (C_{11} = 71.4±0.8, C_{12} = –4.9±1.0, C_{13} = 12.9±0.3, C_{33} = 56.15±0.3, C_{44} = 12.7±0.1 and C_{66} = 6.24±0.05 GPa) and the elastooptic coefficients taken from Ref. [34] (p_{11} = 0.238±0.024, p_{12} = 0.249±0.013, p_{13} = 0.242±0.012, p_{31} = 0.227±0.011, p_{33} = 0.242±0.024, p_{44} = –0.021±0.0021 and p_{66} = –0.068±0.003). All the optical data refer to the light wavelength 632.8 nm.

3. Results and discussions

3.1. Acoustic anisotropy for KDP crystals

As seen from Fig. 1, KDP reveals strong anisotropy of its acoustic properties in the principal crystallographic planes. An interesting feature is that the velocities of the transverse and longitudinal AWs, which propagate in the XY plane along the direction inclined by 45 deg with respect to the principal crystallographic axes a or b, are very close though not equal. This can be understood from the dependences of AW velocities on the AW vector orientation in the XY plane:

$$v_{QT_2}^2(\Theta) = \frac{(C_{11} + C_{66})}{2\rho} - \frac{\sqrt{(C_{11} - C_{66})^2 \cos^2 2\Theta + \sin^2 2\Theta (C_{12} + C_{66})^2}}{2\rho}, \quad (4)$$

$$v_{QT_1}^2(\Theta) = \frac{C_{44}}{\rho}, \quad (5)$$

$$v_{QL}^2(\Theta) = \frac{(C_{11} + C_{66})}{2\rho} + \frac{\sqrt{(C_{11} - C_{66})^2 \cos^2 2\Theta + \sin^2 2\Theta (C_{12} + C_{66})^2}}{2\rho}, \quad (6)$$

where Θ is the angle between the AW vector and the X axis in the XZ plane, i.e. the angle of rotation of the AW vector around the Y axis. Eqs. (6) and (8) are similar in their structure and so the velocities of the AWs QT_2 and QL become approximately equal at Θ = 45 deg, whenever the second term in the r. h. s. of Eqs. (4) and (6) [$(C_{12} + C_{66})/2\rho$] is much smaller than $(C_{11} + C_{66})/2\rho$. The resulting difference between the velocities of the transverse and longitudinal

AWs is about 1.7%. Notice that a similar angular dependence of the AW velocities on the direction of wave propagation has earlier been observed in the TeO_2 crystals [27].

Fig. 1b shows intersections of the indicative acoustic velocity surfaces for the two quasi-transverse AWs propagating at an angles 18.35° + *i*×90° and 71.65° + *i*×90° (*i* = 0, 1, 2, 3) deg to the *X* axis in the principal plane *XY* plane. Note that the velocities of these waves are equal when they propagate along the *Z* axis (see Fig. 1a). Thus, the so-called acoustic axes for the quasi-transverse AWs lie in the four planes which contain the *Z* axis and are rotated around it by the angles mentioned above.

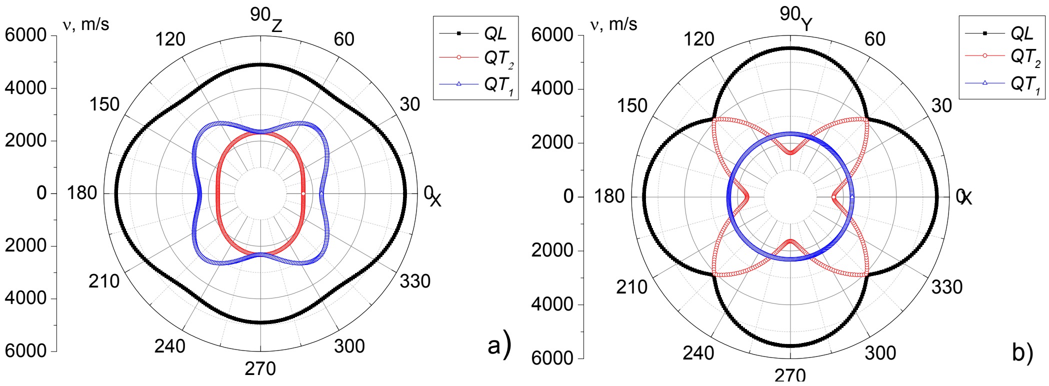

Fig. 1. Dependences of AW velocity on the angular direction Θ of AW propagation, as calculated in the *XZ* (a) and *XY* (b) planes.

We have found that the KDP crystals can manifest significant deviations Δ of the acoustic energy flow from the wave vector (see Fig. 2). In the principal crystallographic plane *XY*, the maximum obliquity for the wave QL amounts to Δ = 37.11 deg and corresponds to the angle Θ = 43 deg with respect to the *X* axis. For the QT_2 and QT_1 waves we have respectively Δ = ±57 deg (*XY* plane; Θ = 16 or 74 deg from the *X* axis) and Δ = –35.4 deg (the *XZ* plane; Θ = 70 deg from the *X* axis). The obliquity angle is equal to zero when the QT_1 wave propagates in the *XY* plane. The group velocities differ for the transverse AWs propagating along the directions that correspond to the acoustic axes, since the obliquity angles are then different (see Fig. 2b). It is worthwhile to note that our results obtained for the *XZ* plane agree well with the data presented in Ref. [35].

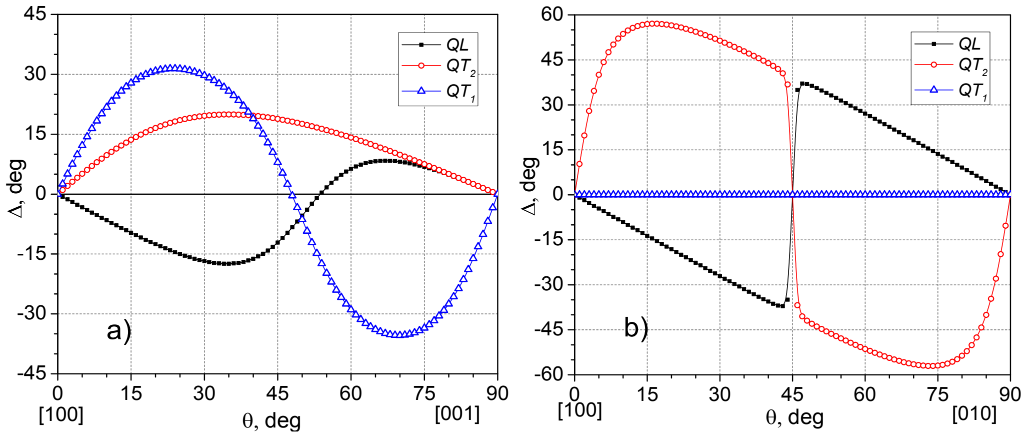

Fig. 2. Dependences of obliquity angle Δ on the direction Θ of AW propagation, as calculated for the *XZ* (a) and *XY* (b) planes.

3.2. Acousto-optic anisotropy for KDP crystals

Let us consider the isotropic AO interaction of the quasi-longitudinal AW $v_{11} = v_{QL}$ propagating in the *XZ* plane with the incident optical wave of which electric displacement vector is given by the ordinary wave polarization (a so-called type I of AO interactions). Fig. 3 shows dependences of the EEC, the AW slowness and the AOFM on the angular orientation Θ_X of the AW vector with respect to the *X* axis. Note that hereafter we accept the condition $\theta_B = 1$ deg for the isotropic diffraction. The maximal AOFM value, 7.01×10^{-15} s^3/kg, is reached for the AO interactions implemented in the *XY* plane ($\varphi_X = 90$ deg) at the angles $\Theta_X = 45$, 135, 225 or 315 deg. This maximum is caused by the maxima found for the EEC and the AW slowness (see Fig. 3a, b).

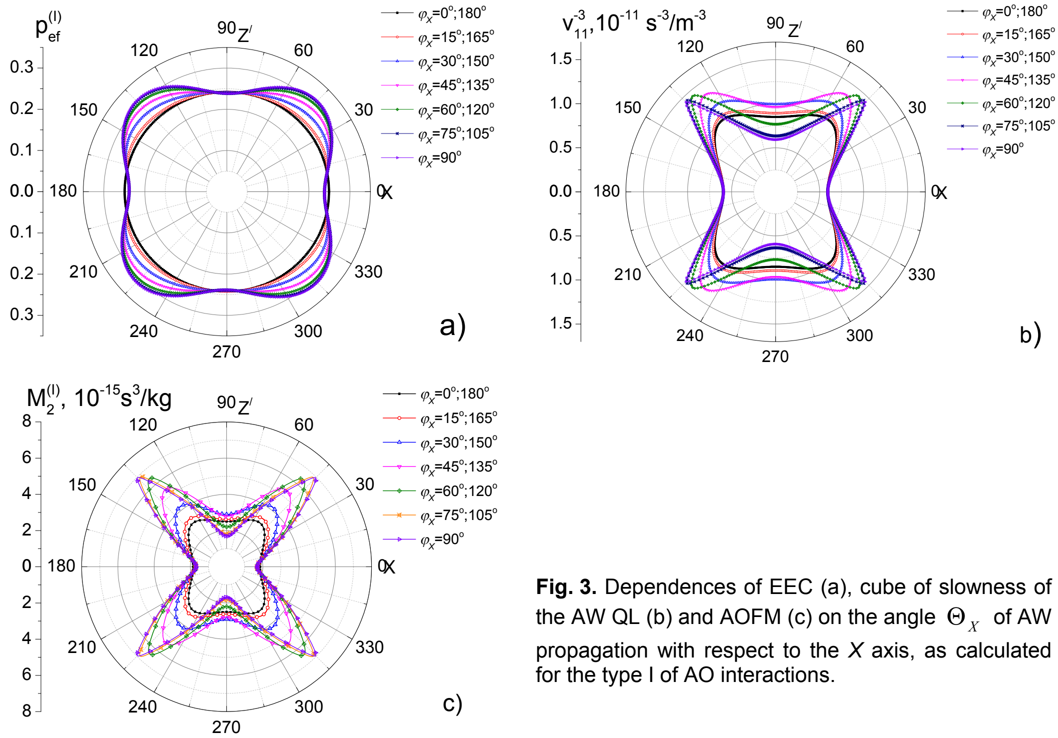

Fig. 3. Dependences of EEC (a), cube of slowness of the AW QL (b) and AOFM (c) on the angle Θ_X of AW propagation with respect to the *X* axis, as calculated for the type I of AO interactions.

For the type II of AO interactions, when the AW QL is coupled with the extraordinary optical wave, the maximal AOFM (3.95×10^{-15} s^3/kg) is reached in the $X'Z$ plane rotated around the *Z* axis by the angle $\varphi_Z = 45$ deg and at $\Theta_X = 0$ or 180 deg (see Fig. 4). It is interesting that, for the both interaction types I and II , the maximal AOFM values concern the same slowest longitudinal AW propagating along the bisector between the *X* and *Y* axes.

As seen from Fig. 5, the maximal AOFM 0.57×10^{-15} s^3/kg for the type III of AO interactions, when the AW QT$_1$ is coupled with the ordinary optical wave, is reached in the *XY* plane ($\varphi_X = 90$ deg) at the angles Θ_X equal to 22, 12, 202 or 292deg. A close AOFM value, $M_2 = 0.53\times 10^{-15}$ s^3/kg, can be reached for the AW propagation direction $\Theta_X = 18$ deg corresponding to intersection of the two surfaces of transverse AWs (see Fig. 1b). The maximal AOFM is due to anisotropy of both the EEC and the AW slowness (see Fig. 5a, b).

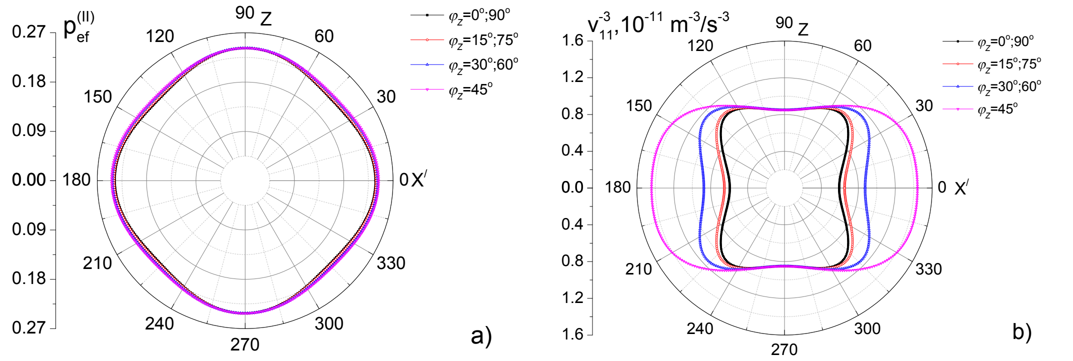

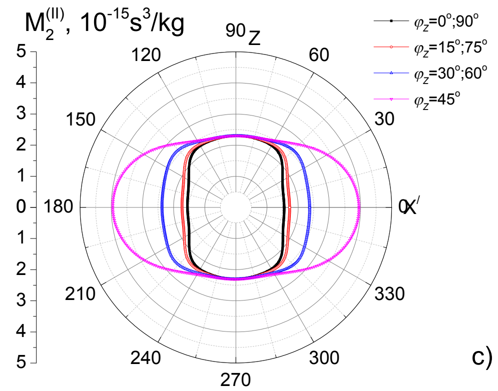

Fig. 4. Dependences of EEC (a), cube of slowness of the AW QL (b) and AOFM (c) on the angle Θ_X of AW propagation with respect to the X' axis, as calculated for the type II of AO interactions with QL AW.

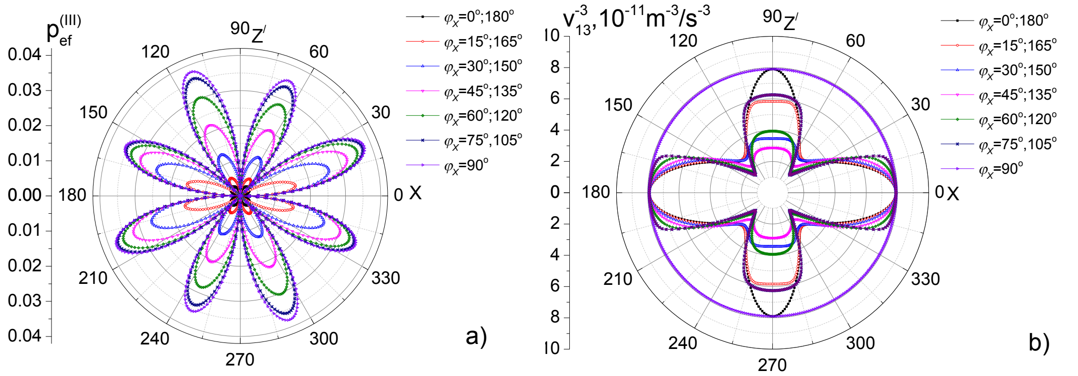

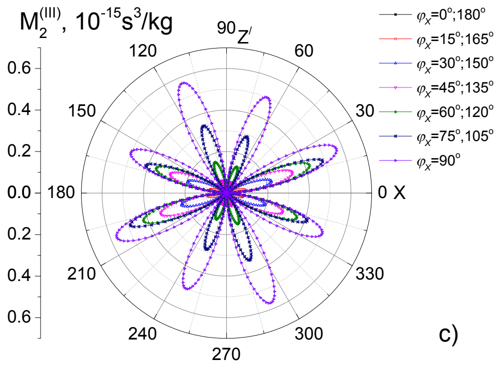

Fig. 5. Dependences of EEC (a), cube of slowness of the AW QT_1 (b) and AOFM (c) on the angle Θ_X of AW propagation with respect to the X axis, as calculated for the type III of AO interactions.

As seen from Fig. 5, the maximal AOFM 0.57×10^{-15} s^3/kg for the type III of AO interactions, when the AW QT_1 is coupled with the ordinary optical wave, is reached in the *XY* plane ($\varphi_X = 90$ deg) at the angles Θ_X equal to 22, 12, 202 or 292deg. A close AOFM value, $M_2 = 0.53 \times 10^{-15}$ s^3/kg, can be reached for the AW propagation direction $\Theta_X = 18$ deg corresponding to intersection of the two surfaces of transverse AWs (see Fig. 1b). The maximal AOFM is due to anisotropy of both the EEC and the AW slowness (see Fig. 5a, b).

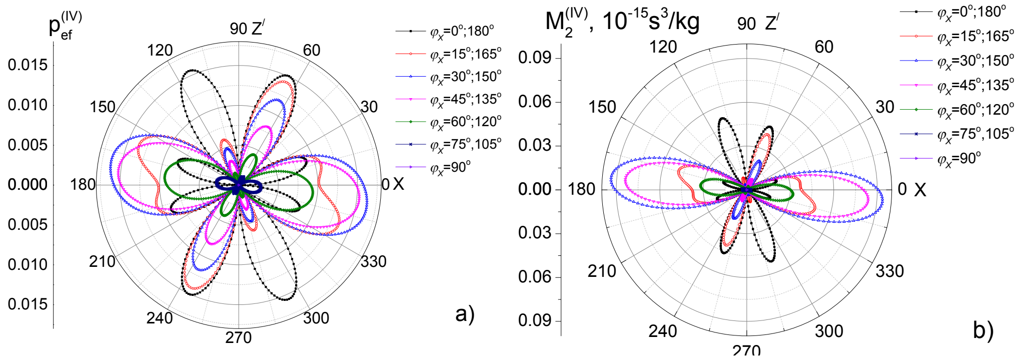

Fig. 6. Dependences of EEC (a) and AOFM (b) on the angle Θ_X of AW propagation with respect to the *X* axis, as calculated for the type IV of AO interactions with the AW QT_1.

The maximal AOFM value 0.09×10^{-15} s^3/kg peculiar for the type IV of AO interactions is achieved in XZ' interaction plane rotated by $\varphi_X = 30$ or 150 deg around the *X* axis. Then the AW QT_1 is coupled with the extraordinary optical wave. As seen from Fig. 6, the AW vector in this plane is inclined by $\theta_X = 175$ or 355 deg with respect to the *X* axis. This AOFM value is mainly due to the EEC anisotropy.

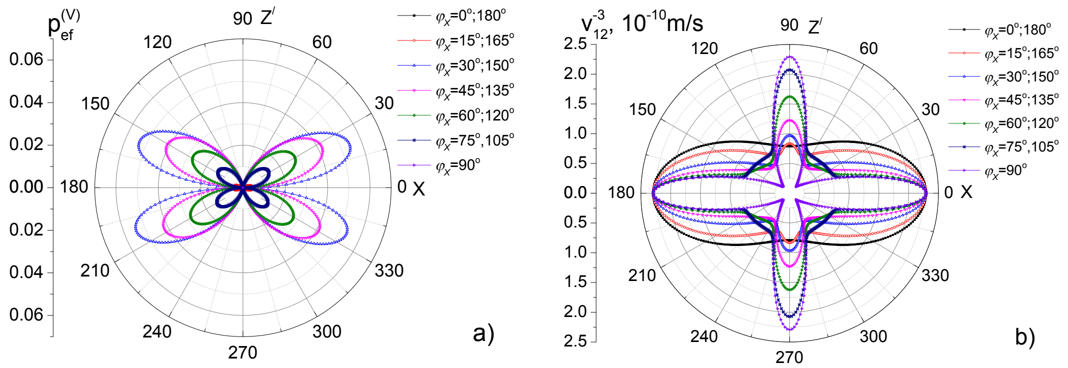

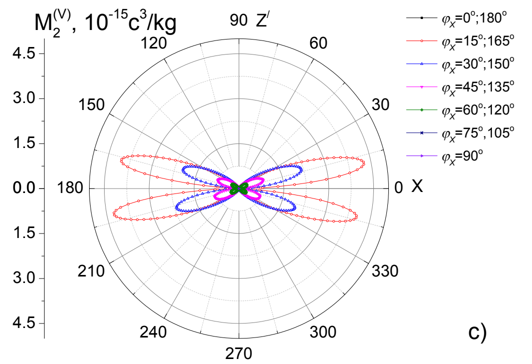

Fig. 7. Dependences of EEC (a), cube of slowness of the AW QT_2 (b) and AOFM (c) on the angle Θ_X of AW propagation with respect to the *X* axis, as calculated for the type V of AO interactions.

When the AW QT_2 interacts with the ordinary optical wave, we deal with the AO interaction type V. Then the maximal AOFM, 4.25×10^{-15} s^3/kg, is reached in the XZ' plane rotated around the X axis by the angles 15 or 165 deg under the condition that the angle Θ_X equals to 12 or 192 deg with respect to the X axis (see Fig. 7). The maximal AOFM value is associated with the maximal EEC. Finally, the type VI of isotropic AO interactions, when the AW QT_2 is coupled with the extraordinary optical wave, is characterized by rather small AOFMs. The maximal value, 0.26×10^{-15} s^3/kg, is achieved in the XZ' plane rotated around the X axis by 60 or 120 deg, under the condition that the angle Θ_X with the X axis is equal to 179 or 359 deg (see Fig. 8).

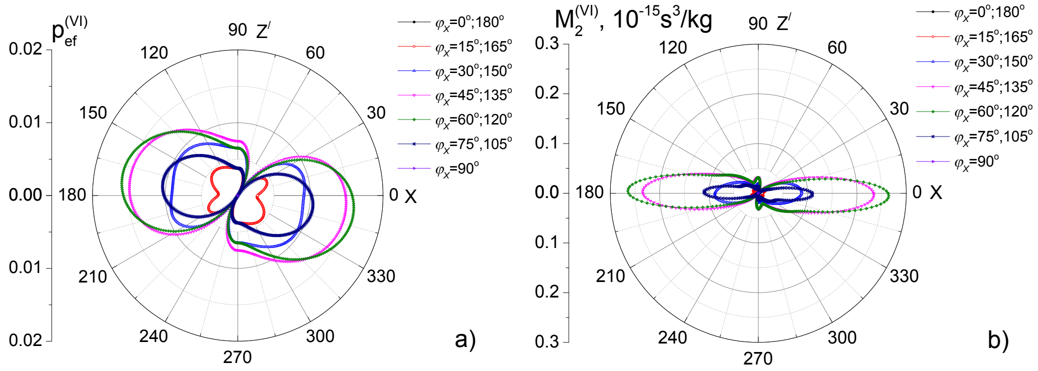

Fig. 8. Dependences of EEC (a) and AOFM (b) on the angle Θ_X of AW propagation with respect to the X axis, as calculated for the type VI of AO interactions with QT_2 AW.

Let us now analyze the anisotropic AO diffraction in the KDP crystals. In case of the type VII of AO interactions with the AW QL, the maximal value of AOFM is equal to 2.58×10^{-15} s^3/kg (see Fig. 9a). This value is achieved in the interaction plane XZ' rotated around the X axis by the angles $\varphi_X = 10$ or 170 deg. The angle of incidence of the optical wave is then equal to $\theta_X = 90$ deg, whereas the diffraction angles are $\gamma = 103$ or 257 deg. The maximal AOFM value for the collinear diffraction at this interaction type is equal to 0.057×10^{-15} s^3/kg. It is reached in the interaction plane XZ' rotated around the X axis by the angles $\varphi_X = 40$ or 140 deg, and at $\theta_X = 50$ or 130 deg.

For the type VIII of interactions, the AOFM is small. The highest AOFM value, 0.15×10^{-15} s^3/kg, is reached in the interaction plane XZ' rotated around the X axis by the angle $\varphi_X = 40$ or 140 deg. Then the angles of incidence are equal to $\theta_X = 40$ or 140 deg, while the diffraction angle is $\gamma = 133$ or 226 deg (see Fig. 9b). The collinear diffraction is characterized by the maximal AOFM value amounting to 0.14×10^{-15} s^3/kg. This AOFM refers to the interaction planes rotated by the angles $\varphi_X = 50$ or 130 deg. The incidence angles in the both cases are equal to $\theta_X = 20$ or 160 deg. As seen from Fig. 8c, the type IX of AO interactions is characterized by the maximal AOFM equal to 5.32×10^{-15} s^3/kg. This value is achieved in the interaction planes XZ and YZ. The incident optical wave under this AO diffraction propagates under the angle $\theta_X = 90$ deg with respect to the X axis, while the diffraction angle is equal to 1 deg. A close value, 5.16×10^{-15} s^3/kg, can be reached in the same interaction plane at $\theta_X = 80$ deg. The maximal AOFM observed at the collinear diffraction amounts to 1.62×10^{-15} s^3/kg. This AOFM is peculiar for the interaction plane XZ and the incidence angles $\theta_X = 40$ or 140 deg.

Table 1. Maximal AOFM values and the corresponding parameters of isotropic AO diffraction in the KDP crystals. Diffracted optical waves propagate under the Bragg angle equal to 1 deg.

Type of AO interaction	AW type and its velocity, m/s	Orientation of the interaction plane, deg	Propagation direction of the AW, deg	Directions of propagation and polarization of the incident optical wave, deg	AW frequency, MHz	AOFM, 10^{-15} s^3/kg
I	QL, 4109.8	$\varphi_X = 90$ (*XY* crystallographic plane)	45; 135; 225 or 315	136, 226, 316 or 46 with respect to the *X* axis; n_o polarization	341.7	7.01
II	QL, 4109.8	$\varphi_Z = 45$	0 or 180	91 or 271 with respect to the X' axis; n_e polarization	341.7	3.95
III	QT_1 2073.5	$\varphi_X = 90$ (XY plane)	22, 112, 202 or 292	113, 203, 293 or 383 with respect to the *X* axis; n_o polarization	172.4	0.57
IV	QT_1 2347.6	$\varphi_X = 30$ or 150	175 or 355	266 or 446 with respect to the *X* axis; n_e polarization	195.2	0.09
V	QT_2 1690.2	$\varphi_X = 15$ or 165	12 or 192	103 or 283 with respect to the *X* axis; n_o polarization	140.5	4.25
VI	QT_2 1635.7	$\varphi_X = 60$ or 120	179 or 359	270 or 90 with respect to the *X* axis; n_e polarization	136.0	0.26

Table 2. Maximal AOFM values and the corresponding parameters of anisotropic AO diffraction in the KDP crystals.

Type of AO interaction	AW type and its velocity, m/s	Orientation of the interaction plane, deg	Propagation direction of the AW, deg	Propagation direction of the incident optical wave, deg	Diffraction angle, deg	AW frequency, MHz	AOFM, 10^{-15} s^3/kg
VII	QL, 4597.5 or 4597.5	$\varphi_X = 10$ or 170	51.5 or 128.5	90	103 or 257	230.3 230.3	2.58
VIII	QT_1, 2476.5 or 3335.7	$\varphi_X = 40$	195.28 or 242.19	40 or 140	133 or 226	269.8 or 270.9	0.15
	QT_1, 3328.12 or 2486	$\varphi_X = 140$	114.5 or 162.18	40 or 140	133 or 226	269.8 or 270.9	0.15
IX	QT_2, 1633.8	$\varphi_Z = 0$ or 90	0.5	90	1	150	5.32

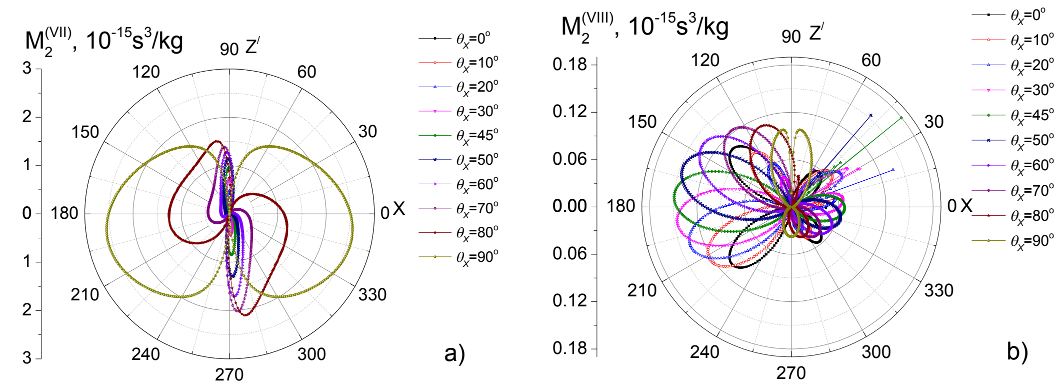

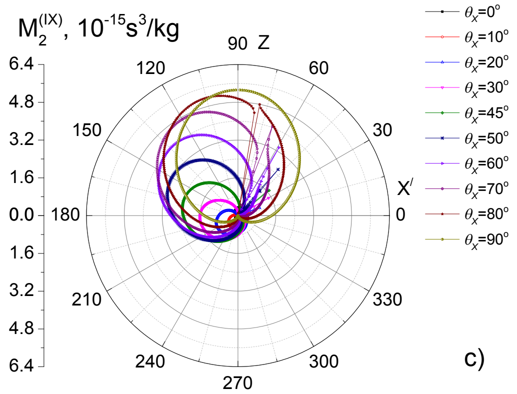

Fig. 9. Dependences of AOFM on $\theta_X + \gamma$ angle, as calculated for the interaction planes where maximal AOFM values are reached for the AO interaction types VII (a), VIII (b) and IX (c).

To compare our results in a systematic manner, we present all of our numeric data in Table 1 and Table 2. The absolute maximum of AOFM is achieved for the isotropic AO interaction of optical waves with the longitudinal AW. Then the AW propagates in the *XY* plane along the bisector of the *X* and *Y* axes. For the case of anisotropic diffraction, the M_2 value is maximal when the optical wave with the incidence angle $\theta_X = 90$ deg interacts with the transverse AW, and the AW propagates close to the *X* axis. Notice that, if one takes dispersion of the refractive indices into account, our results agree well with the experimental data obtained by N. Gupta and V. Voloshynov [11, 12]. The authors of Ref. [11] have considered the AO interactions in the *XZ* plane, when the ordinary optical wave (the wavelength $\lambda = 300$ nm) incident at the angle 12 deg with respect to the *Z* axis is coupled with the AW that propagates along the direction inclined by 6 deg with respect to the *X* axis. For this case they have obtained the parameter $M_2 = 4.6\times10^{-15}$ c^3/kg. Using our data for the same experimental conditions, we arrive at the AOFM equal to 5.5×10^{-15} c^3/kg. The small difference between our results and those reported in Ref. [11] is, most probably, caused by the elastic stiffness coefficients used in our calculations.

4. Conclusion

In the present work we have studied the anisotropy of acoustic properties and the anisotropy of AOFM for the KDP crystals. Basing on the results obtained, we have shown that the maximum AOFM value typical for the case of isotropic AO interaction is equal to $M_2=7.1\times10^{-15}$ s^3/kg. Then the optical wave that propagates along the $[\bar{1}10]$ direction and is polarized in the *XY* plane interacts with the longitudinal AW propagating in the same plane along the $[110]$ direction. For the case of anisotropic AO interactions, the maximum M_2 value is equal to 5.3×10^{-15} s^3/kg. It corresponds to the interaction of slow transverse AW propagating in the *XZ* or *YZ* planes close to the *X* or *Y* axis with the incident optical wave propagating close to the optic axis. The maximal

AOFM obtained under the collinear diffraction is equal to 1.62×10^{-15} s^3/kg. It is peculiar for the interaction of slow shear AW propagating in the *XZ* plane with the optical wave that propagates in the same plane at the angle θ_X = 40 or 140 deg with respect to the *X* axis.

References

1. Fukami T, 1990. Refinement of the crystal structure of KH_2PO_4 in the ferroelectric phase. Phys. Stat. Solidi (a). **117**: K93.
2. Reyné S, Duchateau G, Natoli J-Y and Lamaignère L, 2009. Laser-induced damage of KDP crystals by 1ω nanosecond pulses: influence of crystal orientation. Opt. Express. **17**: 21652–21665.
3. Endert H and Melle W, 1982. Laser-induced damage in KDP crystals. The influence of growth ghosts and growth bands. Phys. Stat. Solidi (a). **74**: 141–148.
4. Mironov S Yu, Ginzburg V N, Lozhkarev V V, Luchinin G A, Kirsanov A V, Yakovlev I V, Khazanov E A and Shaykin A A, 2011. Highly efficient second-harmonic generation of intense femtosecond pulses with a significant effect of cubic nonlinearity. Quant. Electron. **41**: 963–967.
5. Mironov S, Lozhkarev V, Ginzburg V and Khazanov E, 2009. High-efficiency second-harmonic generation of superintense ultrashort laser pulses. Appl. Opt. **48**: 2051–2057. https://doi.org/10.1364/AO.48.002051
6. Zhu H, Wang T, Zheng W, Yuan P and Qian L, 2004. Efficient second harmonic generation of femtosecond laser at 1 μm. Opt. Expess. **12**: 2150–2155.
7. Aoyama M, Harimoto T, Ma J, Akahane Y and Yamakawa K. 2001, Second-harmonic generation of ultra-high intensity femtosecond pulses with a KDP crystal. Opt. Express. **9**: 579–585.
8. http://www.inradoptics.com/pdfs/Inrad_AN__FemtosecondTiSapphSHG.pdf
9. Coudreau S, Kaplan D and Tournois P, 2006. Ultraviolet acousto-optic programmable dispersive filter laser pulse shaping in KDP. Opt. Lett. **31**: 1899–1901.
10. Dekemper E, Fussen D, Van Opstal B, Vanhamel J, Pieroux D, Vanhellemont F, Mateshvilia N, Franssens G, Voloshinov V, Janssen C and Elandaloussi H, 2014. ALTIUS: a spaceborne AOTF-based UV-VIS-NIR hyperspectral imager for atmospheric remote sensing. Proc. SPIE. **9241**: 92410L-1–92410L-10.
11. Gupta N and Voloshinov V, 2004. Hyperspectral imager, from ultraviolet to visible, with a KDP acousto-optic tunable filter. Appl. Opt. **43**: 2752–2759.
12. Gupta N and Voloshinov V, 2014. Spectral characterization in deep UV of an improved imaging KDP acousto-optic tunable filter. J. Opt. **16**: 035301–035310 .
13. Hov O, Tropospheric ozone research: ozone in the regional and sub-regional context. Berlin: Springer (1997).
14. Gupta L, Sharma R C, Razdan A K and Maini A K, 2014. Laser induced fluorescence of biochemical for UV LIDAR application. J. Fluoresc. **24**:709–711.
15. David G, Thomas B, Dupart Y, D'Anna B, George C, Miffre A and Rairoux P, 2014. UV polarization lidar for remote sensing new particles formation in the atmosphere. Opt. Express. **22**: A1009–A1022.
16. Shibata T, Fukuda T, Narikiyo T and Maeda M, 1987. Evaluation of the solar-blind effect in ultraviolet ozone lidar with Raman lasers. Appl. Opt. **26**: 2604–2608.
17. Wolfram E, Salvador J, Orte F, Delia R and Quel E, 2012. Systematic ozone and solar UV measurements in the observatorio atmosférico de la Patagonia Austral, Argentina. Revista Boliviana de Física. **20**: 13–15.

18. Zhang J, Wang S, Fang C, Sun X, Gu Q, Li Y, Wang B, Liu B and Mu X, 2007. Growth habit and transparency of sulphate doped KDP crystal. Mater. Lett. **61**: 2703–2706.
19. Mys O, Kostyrko M, Smyk M, Krupych O and Vlokh R, 2014. Anisotropy of acoustooptic figure of merit in optically isotropic media. Appl. Opt. **53**: 4616–4627.
20. Mys O, Kostyrko M, Smyk M, Krupych O and Vlokh R, 2014. Anisotropy of acoustooptic figure of merit for TeO_2 crystals. 1. Isotropic diffraction. Ukr. J. Phys. Opt. **15**: 132–154.
21. Mys O, Kostyrko M, Krupych O and Vlokh R, 2014. Anisotropy of acoustooptic figure of merit for TeO_2 crystals. 2. Anisotropic diffraction. Ukr. J. Phys. Opt. **16**: 38–60.
22. Martynyuk-Lototska I, Mys O, Dudok T, Adamiv V, Smirnov Y and Vlokh R, 2008. Acousto-optic interaction in α-BaB_2O_4 and $Li_2B_4O_7$ crystals. Appl. Opt. **47**: 3446–3454.
23. Mys O, Krupych O, Kostyrko M and Vlokh R, 2016. Anisotropy of acousto-optic figure of merit for $LiNbO_3$ crystals: anisotropic diffraction. Erratum. Appl. Opt. **55**: 9823–9829.
24. Mys O, Kostyrko M, Krupych O and Vlokh R, 2015. Anisotropy of the acousto-optic figure of merit for $LiNbO_3$ crystals: isotropic diffraction. Appl. Opt. **54**: 8176–8186.
25. Mys O, Krupych O and Vlokh R, 2016. Anisotropy of an acousto-optic figure of merit for $NaBi(MoO_4)_2$ crystals. Appl. Opt. **55**: 7941–7955.
26. Pyle J R, 1966. Laser modulation using linear electro-optic crystals. Tech. Note PAD 125, 35 p. NASA N67–27128.
27. Shaskolskaya M P, Acoustic crystals. Moscow: Nauka, 1982.
28. Mys O, Kostyrko M, Vasylkiv Yu and Vlokh R, 2015. Anomalous behaviour of acoustooptic figure of merit under the conditions of collinear diffraction. Ukr. J. Phys. Opt. **16**: 179–183.
29. Smith T and Korpel A, 1965. Measurement of light-sound interaction efficiencies in solids. IEEE J. Quant. Electron. **1**: 283–284.
30. Bystrova T G and Fedorov F I, 1968. Debye temperatures of tetragonal and trigonal crystals. Sov. Phys.: Crysallogr. **12**: 493–498.
31. Balakshyi V I, Paryhyn V N and Chyrkov L E. Basic physics of acoustooptics. Moscow: Radio and Communications, 1985.
32. Ohmachi Y, Uchida N and Niizeki N, 1972. Acoustic wave propagation in TeO_2 single crystal. Journ. Acoust. Soc. Amer. **51**: 164–168.
33. Price W J and Huntington H B, 1950. Acoustical properties of anisotropic materials. Journ. Acoust. Soc. Amer. **22**: 32–37.
34. Avakyants L P, Kiselev D F, Perelomova N V, Sugrej V I, 1983. Elastooptics of KH_2PO_4, KD_2PO_4 and RbH_2PO_4. Fiz. Tverd. Tela. **25**: 580–582.
35. Molchanov V, Chizhikov S and Makarov O, 2008. Quasicollinear acoustooptic tunable filters based on KDP single crystal. Intern. Conf. Acoustics_08: 827–831.

Mys O., Krupych O. and Vlokh R. 2017. Anisotropy of acoustooptic figure of merit in KH_2PO_4 crystals. Ukr.J.Phys.Opt. **18**: 83 – 94.

Анотація. *У роботі проаналізовано анізотропію коефіцієнта акустооптичної якості кристалів KH_2PO_4. Показано, що найвище значення цього коефіцієнта (7.1×10^{-15} $с^3$/кг) досягається при ізотропній акустооптичній взаємодії поляризованої в площині XY оптичної хвилі, яка поширюється вздовж напрямку* $[\bar{1}10]$, *із поздовжньою акустичною хвилею, яка поширюється в цій же площині в напрямку* $[110]$. *У разі анізотропної дифракції максимальне значення коефіцієнта M_2 менше (5.3×10^{-15} $с^3$/кг) і відповідає взаємодії повільної поперечної акустичної хвилі, яка поширюється в площинах XZ або YZ у напрямку близькому до осі X, з оптичною хвилею, яка поширюється майже вздовж оптичної осі кристала.*